Accurate reaction paths using a Hessian based predictor–corrector integrator

Hrant P. Hratchian and H. Bernhard Schlegel[a)]
Department of Chemistry and Institute for Scientific Computing, Wayne State University, Detroit, Michigan 48202

(Received 11 December 2003; accepted 8 March 2004)

Central to the theoretical description of a chemical reaction is the reaction pathway. The intrinsic reaction coordinate is defined as the steepest descent path in mass weighted Cartesian coordinates that connects the transition state to reactants and products. In this work, a new integrator for the steepest descent pathway is presented. This method is a Hessian based predictor–corrector algorithm that affords pathways comparable to our previous fourth order method at the cost of a second order approach. The proposed integrator is tested on an analytic surface, four moderately sized chemical reactions, and one larger organometallic system. © *2004 American Institute of Physics.* [DOI: 10.1063/1.1724823]

I. INTRODUCTION

In the theoretical study of a chemical reaction, the reaction pathway plays an integral role. Typically, one employs reaction path following calculations to ensure that a transition state (TS) found on a particular potential energy surface (PES) lies on a pathway that connects the two intended PES minima. Reaction pathways are also used to derive an accurate description of the PES along the minimum energy path (MEP) to compute rate constants via variational transition state theory (VTST) or reaction path Hamiltonian (RPH) formalisms.[1–5]

There are two basic varieties of reaction path procedures. The first type, often referred to as pathway optimization methods, search for a reaction path without prior knowledge of the TS and are commonly used to simultaneously find a TS and the reaction pathway. The second type begins at a previously optimized TS and follows paths down to the reactant and product wells. Although pathway optimization methods have gained much attention in recent years, they require multiple points or images along an interpolated pathway. These images are minimized in a constrained and concerted way, and thus usually require a large number of energy and derivative calculations. A recent implementation of nudged elastic band methods in Gaussian-based *ab initio* electronic structure codes required between 50 and 201 gradient calculations (with a relatively low density of images) to describe the isomerization reaction of HCN→HNC.[6] Obviously, these approaches are particularly ill suited for those cases where a very accurate path is needed in the area near the TS, as with VTST and RPH, for even modest sized systems. In this work, we focus our discussion exclusively on the second type of reaction path algorithm—those that begin at a user supplied TS and trace the two pathways (forward and reverse) that lead to reactants and products.

Beginning at a first-order saddle point on the PES, which corresponds to a TS, the reaction pathway can be determined by following the steepest descent path downhill in both directions. The steepest descent pathway is given by the differential equation

$$\frac{d\mathbf{x}(s)}{ds} = -\frac{\mathbf{g}(\mathbf{x})}{|\mathbf{g}(\mathbf{x})|}, \tag{1}$$

where s is the arc length along the path, $\mathbf{x}$ is the vector of Cartesian coordinates, and $\mathbf{g}$ is the PES gradient at $\mathbf{x}$. Some care must be taken when integrating the steepest descent pathway as Eq. (1) corresponds to a stiff differential equation. Although a steepest descent path can be obtained in any coordinate system, when mass-weighted Cartesian coordinates are used the steepest descent path is known as the intrinsic reaction coordinate (IRC).[7]

A multitude of approaches to reaction path following are present in the literature and have been extensively reviewed.[8–23] In general, a reaction path following algorithm may be classified as either explicit or implicit. Explicit methods take each step using derivative information only at the starting point; implicit methods take each step using derivative information at both the starting and end points. Common explicit algorithms include Euler's method, the Ishida–Morokuma–Komornicki (stabilized Euler) method,[12,13] Runge–Kutta,[14,15] the local quadratic approximation (LQA),[16,17] and the Sun–Ruedenberg modification of LQA.[19] Some of these methods require only gradient information and are limited to rather small step sizes, while others also use second derivatives (the Hessian). Methods that use the Hessian are more costly, but gain additional stability allowing for somewhat larger step sizes.

Implicit methods for differential equations are more difficult to implement because the gradient, and possibly higher order derivatives, are necessary at the end of the step. Since these methods generally require the use of optimization schemes at each step to iteratively solve for the derivatives at the end point,[24] they tend to require multiple energy and derivative calculations for each step. However, implicit

a)Author to whom correspondence should be addressed; Electronic mail: hbs@chem.wayne.edu

methods are often able to take considerably larger steps than explicit methods allowing them to compensate for these additional derivative calculations. Implicit methods for IRC analysis include the Müller–Brown (implicit Euler) method,[18] the second order Gonzalez and Schlegel (implicit trapezoid) method,[20,21] and higher order methods by the same authors.[22]

In this paper, we introduce a new explicit integration scheme to solve Eq. (1). This new approach uses a Hessian based predictor-corrector (HPC) integrator that aims to solve the pathway with a high degree of accuracy. The present algorithm has been designed with the hope of developing an approach that is well suited for use in VTST and RPH calculations where an accurate description of the reaction path is essential. Since analytic Hessians are necessary at points along the path for computing path curvatures, coupling matrix elements and projected frequencies for VTST and RPH calculations, our method makes use of second derivatives at each step.

II. METHOD

The present algorithm makes use of a Hessian based predictor–corrector integrator. Related algorithms[25,26] have been found to be quite efficient for integrating *ab initio* classical trajectory calculations. The LQA integrator of Page and McIver[16] is used for the predictor steps, and a modified Bulirsch–Stoer integrator[27–29] is used on a fitted distance weighted interpolant (DWI) surface[30–32] for the corrector steps. The fitted surface is a two point DWI surface that employs positions, energies, gradients, and Hessians at the start and end points from the predictor integration. After each corrector integration is complete, the DWI gradient at the corrected end point and the Hessian from the predicted end point are used for the next LQA step. In this way, each step along the reaction path requires only one computation of the energy and its first and second derivatives. Thus, the corrector step adds no additional electronic structure calculations to a standard LQA calculation.

A. Local quadratic approximation for the predictor step

The LQA integrator is based upon a second order Taylor series of the PES, and was introduced by Page and McIver.[16,17] Truncated at the quadratic term, the Taylor series expansion of the PES about $\mathbf{x_0}$ is given by

$$E(\mathbf{x}) = E_0 + \mathbf{g_0^t}\Delta\mathbf{x} + \tfrac{1}{2}\Delta\mathbf{x^t}\mathbf{H_0}\Delta\mathbf{x}, \tag{2}$$

where $\Delta\mathbf{x}$, $\mathbf{g_0}$, and $\mathbf{H_0}$ are the displacement vector of the current position from $\mathbf{x_0}$, the gradient, and Hessian at $\mathbf{x_0}$, respectively. Taking the first derivative of Eq. (2) with respect to $\Delta\mathbf{x}$ gives the gradient as

$$\mathbf{g(x)} = \mathbf{g_0} + \mathbf{H_0}\Delta\mathbf{x}. \tag{3}$$

Substituting Eq. (3) into Eq. (1) gives

$$\frac{d\mathbf{x}(s)}{ds} = -\frac{\mathbf{g_0} + \mathbf{H_0}\Delta\mathbf{x}}{|\mathbf{g_0} + \mathbf{H_0}\Delta\mathbf{x}|}. \tag{4}$$

In the LQA method of Page and McIver, Eq. (4) is integrated by introducing an independent parameter, t, such that

$$\frac{ds}{dt} = |\mathbf{g_0} + \mathbf{H_0}\Delta\mathbf{x}| \tag{5}$$

and

$$\frac{d\mathbf{x}}{dt} = -[\mathbf{g_0} + \mathbf{H_0}\Delta\mathbf{x}]. \tag{6}$$

The solution to Eq. (6) is given by

$$\mathbf{x}(t) = \mathbf{x_0} + \mathbf{A}(t)\mathbf{g_0}, \tag{7}$$

where

$$\mathbf{A}(t) = \mathbf{U}\alpha(t)\mathbf{U^t}. \tag{8}$$

In Eq. (8), $\mathbf{U}$ is the matrix of column eigenvectors of the Hessian and $\alpha(t)$ is a diagonal matrix given by

$$\alpha_{ii}(t) = (e^{-\lambda_i t} - 1)/\lambda_i, \tag{9}$$

where λ_i are the eigenvalues of the Hessian.

In order to integrate Eq. (4), one must obtain a value of t such that the user's desired step size $(s - s_0)$ is taken. To accomplish this, iterations over successive Euler integrations of Eq. (5) are used. The initial value for the Euler step size, δt, is estimated by

$$\delta t = \frac{1}{N_{\text{Euler}}}\frac{(s - s_0)}{|\mathbf{g_0}|}, \tag{10}$$

where N_{Euler} is the number of Euler steps to be taken. In the present implementation, $N_{\text{Euler}} = 5000$. The numerical integration of Eq. (5) can be carried out readily in the Hessian eigenvector space,

$$\frac{ds}{dt} = \left(\sum_i g_{0i}'^2 e^{-2\lambda_i t}\right)^{1/2} \tag{11}$$

where

$$\mathbf{g_0'} = \mathbf{U^t}\mathbf{g_0}. \tag{12}$$

At the start of the integration, when $\mathbf{x}$ corresponds to the TS, the gradient is zero and hence the transition vector must be used in place of $\mathbf{g_0}$. At the TS, the LQA step is equivalent to the gradient extremal step, as described by Hoffman, Nord, and Ruedenburg.[33] At the end of the LQA integration, when $\mathbf{x}$ approaches the minimum wells of the reactant and product, t heads to infinity and the LQA step is equivalent to a Newton–Raphson step, which leads to the minimum energy structure in the local quadratic region. For this reason, conservation of the desired step size, $(s - s_0)$, becomes difficult in this region.

B. Modified Bulirsch–Stoer algorithm for the corrector step

The Bulirsch–Stoer integrator is very well described elsewhere.[24,27–29,34] Here, we provide only an overview of the method and discuss modifications made to the standard algorithm.

Each Bulirsch–Stoer step is comprised of three basic components. First, a simple gradient based integrator is used

to take multiple steps along the Bulirsch–Stoer step interval. In general, this integrator is modified midpoint; however, in our tests we found that the stiff character of Eq. (1) is greatly magnified by the modified midpoint method (see below). This result is consistent with data previously presented by Melissas and co-workers.[35] Therefore, our modified version employs simple Euler integration. At the TS, where the magnitude of the gradient is zero, the step direction is taken to be parallel to the transition vector. The second component of a Bulirsch–Stoer step is to describe the solution of the Euler integration as a polynomial function of step size and to extrapolate to a step size of zero (corresponding to the case where an infinite number of steps are taken). The third component consists of evaluating the error of the extrapolation. If the error is too large, the process is repeated using more steps in the Euler integration, which in turn provides one more data set for the polynomial extrapolation. If the error is acceptable ($<1\times10^{-6}$ a.u. in the present case), then the extrapolated solution to Eq. (1) is accepted, the integration is considered complete, and the next predictor step is taken using the corrected position and gradient.

It should be noted that a semi-implicit Bulirsch–Stoer methodology has been described for handling stiff differential equations that are difficult for the standard integrator to propagate. This semi-implicit form requires first derivatives of the right-hand side of Eq. (1) at every step in the integration; however, in the present form of the DWI surface such derivatives are not trustworthy and the use of the semi-implicit Bulirsch–Stoer integrator is unfeasible.

C. Euler versus modified midpoint integration in the corrector step

To gain some understanding of the difficulties encountered by the standard Bulrisch–Stoer integrator, we explored the cause of the instability of modified midpoint integration of Eq. (1).

It is quite surprising that simple Euler integration is able to accurately integrate Eq. (1) while modified midpoint is not, given the higher formal order of the modified midpoint algorithm. The root of this counterintuitive result is assumed to be the stiff nature of Eq. (1). A stiff differential equation, as described by Gear,[24] results when the rates of decay of coupled equations are significantly different. In the case of Eq. (1), the rate of decay of the true solution (i.e., the IRC) is in competition with the rate of decay of the error in the path that arises when the current point lies off of the pathway. This second numerical solution to Eq. (1) produces a pathway that runs perpendicular to the true IRC. In practice, the solution that one obtains will result from a linear combination of these two solutions. The degree of influence on the integration by the second (erroneous) solution is chiefly dependent upon the deviation of the current point from the true solution and the ratio of the magnitude of the force constant in the direction perpendicular to the IRC and the magnitude of the force parallel to the IRC.

To illustrate this point we begin by studying the forms of the two integrators considered. Given a differential equation

$$\frac{dy}{dx}=f(x,y)\,, \tag{13}$$

the Euler integrator solves for each successive point, y_i, according to

$$y_i=y_{i-1}+\Delta x\cdot f(x,y_i). \tag{14}$$

Modified midpoint integration begins by computing

$$y_1=y_0+\Delta x\cdot f(x,y_0). \tag{15}$$

Subsequent steps are given by a leapfrog method,

$$y_n=y_{n-2}+2\Delta x\cdot f(x,y_{n-1}). \tag{16}$$

To investigate the relative stability [i.e., the ability of the method to follow the true IRC as opposed to the erroneous pathway arising from the stiff nature of Eq. (1)] of each integrator, we have considered a simple two-dimensional harmonic trough potential,

$$E(x,y)=-ax+by^2. \tag{17}$$

For this surface, the first and second derivatives are given by

$$\mathbf{g}=(-a,by),\quad \mathbf{H}=\begin{bmatrix}0 & 0\\ 0 & b\end{bmatrix}. \tag{18}$$

Euler integration of Eq. (1) gives each point in the path, (x_i,y_i) according to

$$x_i=x_{i-1}-\Delta s\,\frac{-a}{\sqrt{a^2+(by_{i-1})^2}},$$

$$y_i=y_{i-1}-\Delta s\,\frac{by_{i-1}}{\sqrt{a^2+(by_{i-1})^2}}. \tag{19}$$

Modified midpoint integration gives the first step as

$$x_1=x_0-\Delta s\,\frac{-a}{\sqrt{a^2+(by_0)^2}},\quad y_1=y_0-\Delta s\,\frac{by_0}{\sqrt{a^2+(by_0)^2}} \tag{20}$$

and subsequent steps as

$$x_i=x_{i-2}-2\Delta s\,\frac{-a}{\sqrt{a^2+(by_{i-1})^2}},$$

$$y_i=y_{i-2}-2\Delta s\,\frac{by_{i-1}}{\sqrt{a^2+(by_{i-1})^2}}. \tag{21}$$

Integration results using both methods on the two-dimensional harmonic trough potential for arbitrary values for a, b, and step size are shown in Fig. 1. Figure 1(b) also pictorially describes the leapfrog nature of the modified midpoint steps for finding $\mathbf{x}_i$ for $i>1$ [Eq. (21)].

To determine the critical step size that results in continuous oscillation across the true IRC, we begin by letting the initial point have a lateral error such that $y_0>0$. Euler integration of the harmonic trough potential develops continuous oscillation of the integrated pathway when a step is taken that crosses the IRC and goes to a point on the opposite side

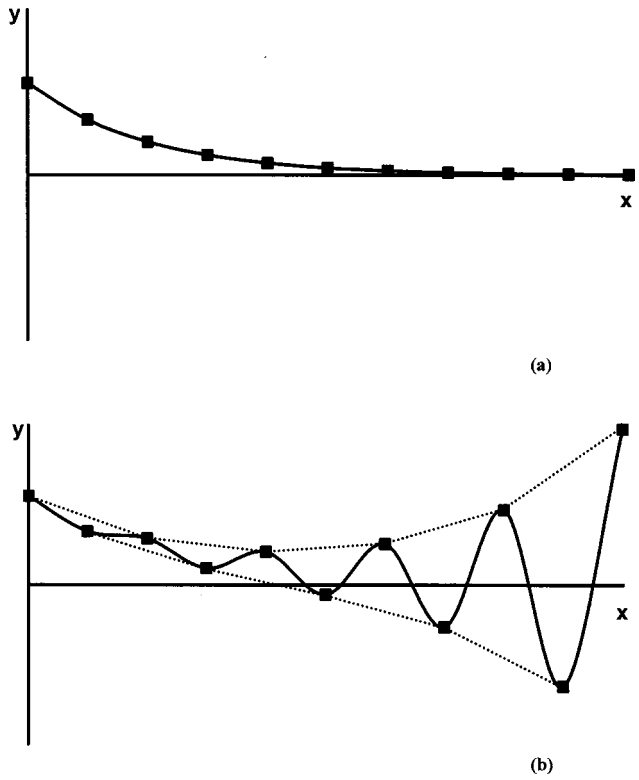

FIG. 1. Reaction path following on the harmonic trough potential, $E(x,y) = -ax+by^2$, using (a) Euler integration and (b) modified midpoint. Pathways are started from a position displaced from the path in the vertical direction by Δy. The leapfrog character of modified midpoint is shown with dotted lines connecting $\mathbf{x}_i$ and $\mathbf{x}_{i-2}$.

of the path that has equal or greater lateral error, $-y_i \geqslant y_{i-1}$ for $y_{i-1}>0$. Solving for the step size that yields oscillation gives

$$\Delta s \geqslant 2\sqrt{\frac{a^2}{b^2}+y_{i-1}^2}. \tag{22}$$

The leapfrog character of modified midpoint integration will cause oscillation when the integrator simply crosses the IRC, $y_i<0$. On the first step, the step size that will yield oscillation is

$$\Delta s > \sqrt{\frac{a^2}{b^2}+y_0^2}. \tag{23}$$

For subsequent steps (i.e., $\mathbf{x}_{i-2}\rightarrow\mathbf{x}_i$), the step size that will yield oscillation is

$$\Delta s > \frac{y_{i-2}}{2y_{i-1}}\sqrt{\frac{a^2}{b^2}+y_{i-1}^2}. \tag{24}$$

This analysis shows, that given a step size, Δs, and small lateral error the modified midpoint integrator is much more likely than the Euler integrator to fall into an erroneous solution to Eq. (1) and to produce continuous and/or growing oscillations perpendicular to the IRC.

D. Distance weighted interpolants

The modified Bulirsch–Stoer integrator requires a large number of energy and gradient evaluations and can be quite costly if energies and derivatives are required from electronic structure methods. However, in the present algorithm the Bulirsch–Stoer integration is carried out on a surface that is fitted to energy and derivative information already available from the predictor step (LQA). Once the Bulirsch–Stoer integration is completed and the LQA end point is corrected, the gradient on the fitted surface is used to take the next LQA predictor step. Since the corrected end point and predicted end point are expected to lie within the same quadratic region of the PES, the Hessian from the previous predictor end point is used for the next LQA step. The validity of this assumption has been demonstrated in previous work on the integration of *ab initio* classical trajectories using a Hessian based predictor–corrector algorithm.[25,26]

In the current algorithm, the Bulirsch–Stoer integration is carried out on a DWI surface, such as those described by Collins and co-workers.[32,36–38] DWI surfaces have been used in conjunction with a number of varying applications.[39] Furthermore, DWI surfaces have been used in multiple dynamics applications and are very well suited for modeling chemical PESs (see Ref. 28 for an overview). The general DWI surface gives the interpolated energy, E_{DWI}, according to

$$E_{\mathrm{DWI}}=\sum_{i=1}^{n} w_i T_i, \tag{25}$$

where the summation is taken over a collection of n points on the PES about which n Taylor series are evaluated and added together in a weighted fashion, which is defined by the weighting functions w_i. In the present implementation, we consider the case where $n=2$, corresponding to the predictor step's starting point and end point.

The Taylor expansions used in Eq. (25) have been truncated after second order terms giving

$$T_i(\Delta\mathbf{x}_i)=E_i+\mathbf{g}_i^t\Delta\mathbf{x}_i+\tfrac{1}{2}\Delta\mathbf{x}_i^t\mathbf{H}_i\Delta\mathbf{x}_i, \tag{26}$$

where

$$\Delta\mathbf{x}_i=\mathbf{x}-\mathbf{x}_i. \tag{27}$$

The weighting functions used have the form

$$w_i=\frac{1}{|\Delta\mathbf{x}_i|^2}\left(\sum_{j=1}^{n}\frac{1}{|\Delta\mathbf{x}_j|^2}\right)^{-1}. \tag{28}$$

Algebraic simplification provides a more computationally convenient form for Eq. (28) that prevents division by zero.

$$w_1=\frac{|\Delta\mathbf{x}_2|^2}{|\Delta\mathbf{x}_1|^2+|\Delta\mathbf{x}_2|^2},\quad w_2=\frac{|\Delta\mathbf{x}_1|^2}{|\Delta\mathbf{x}_1|^2+|\Delta\mathbf{x}_2|^2}. \tag{29}$$

DWI energy and gradient calculations require $O(N^2)$ operations. However, in the context of semi empirical, *ab initio*, and post SCF methods, where the calculation of the potential energy and formation of PES derivatives will be the computational bottleneck, these calculations are essentially free. The prognosis, though, will not be so favorable when molecular mechanics PESs are utilized. Approaches to make the present algorithm more efficient for use with molecular mechanics and QM/MM methods, for instance sparse methods, will be considered in future work.

III. APPLICATIONS

The present algorithm has been tested on one analytic surface and implemented in the development version of GAUSSIAN 03[40] for testing on five chemical PESs. The analytic potential considered is the Müller–Brown (MB) surface. The five chemical systems studied are HCN→HNC, a Diels–Alder reaction, $CH_3CH_2F \rightarrow CH_2CH_2 + HF$, $Cl^- + CH_3Cl \rightarrow ClCH_3 + Cl^-$, and a metallacycle formation reaction. For integrations on chemical systems, 1 a.u. along the path corresponds to a step size of 1 bohr amu$^{1/2}$.

A. Müller–Brown surface

The MB surface[18] provides an excellent test case for reaction path following methods. The MB surface is given by

$$E(x,y) = \sum A_i \exp[a_i(x_i - x_i^0)^2 + b_i(x_i - x_i^0)(y_i - y_i^0) + c_i(y_i - y_i^0)^2], \quad (30)$$

where $A = \{-200, -100, -170, 15\}$, $x^0 = \{1, 0, -0.5, -1\}$, $y^0 = \{0, 0.5, 1.5, 1\}$, $a = \{-1, -1, -6.5, 0.7\}$, $b = \{0, 0, 11, 0.6\}$, and $c = \{-10, -10, -6.5, 0.7\}$. Figure 2 shows the contour plot of this surface and the reaction pathway (shown as a solid line), which was computed using Euler integration with a small step size (0.0001). The TS is at $(-0.822, 0.624)$ and the minimum considered here is at $(-0.558, 1.442)$. Because the reaction path is curved, this surface is challenging to reaction path following integrators when large step sizes are used. As a result, this surface has often been used to test new methods.

Figure 2(a) shows LQA pathways using step sizes ranging from 0.05 to 0.20. The smallest step size yields a pathway that follows the true reaction path very well. However, at a step size of 0.10 the LQA path begins to deviate from the true path at the sharp curve. The rms perpendicular distance between this pathway and the Euler path is 0.0043. Using a step size of 0.20 (largest step size considered here), the LQA path takes the reaction path curve very wide and the rms perpendicular distance to the Euler pathway is 0.018. Although the LQA path rejoins the true path soon after the curve, it fails to accurately describe the reaction path near the TS, where it is most necessary for applications using VTST or RPH.

Figure 2(b) shows pathways computed on the same surface with the same step sizes using the HPC algorithm presented for the first time in this work. As with the LQA pathways, the HPC pathways do an excellent job of following the true reaction pathway when small steps are taken. Unlike LQA, though, the HPC integrator is also capable of following the true reaction path when larger step sizes are used. Indeed, with a step size of 0.20 the rms perpendicular distance between the HPC and Euler paths is 0.0038, nearly five times smaller than that for the corresponding LQA pathway. Thus, the HPC method provides an excellent description of the reaction path around the curve and satisfies the requirement of providing accurate integration of Eq. (1) near the TS.

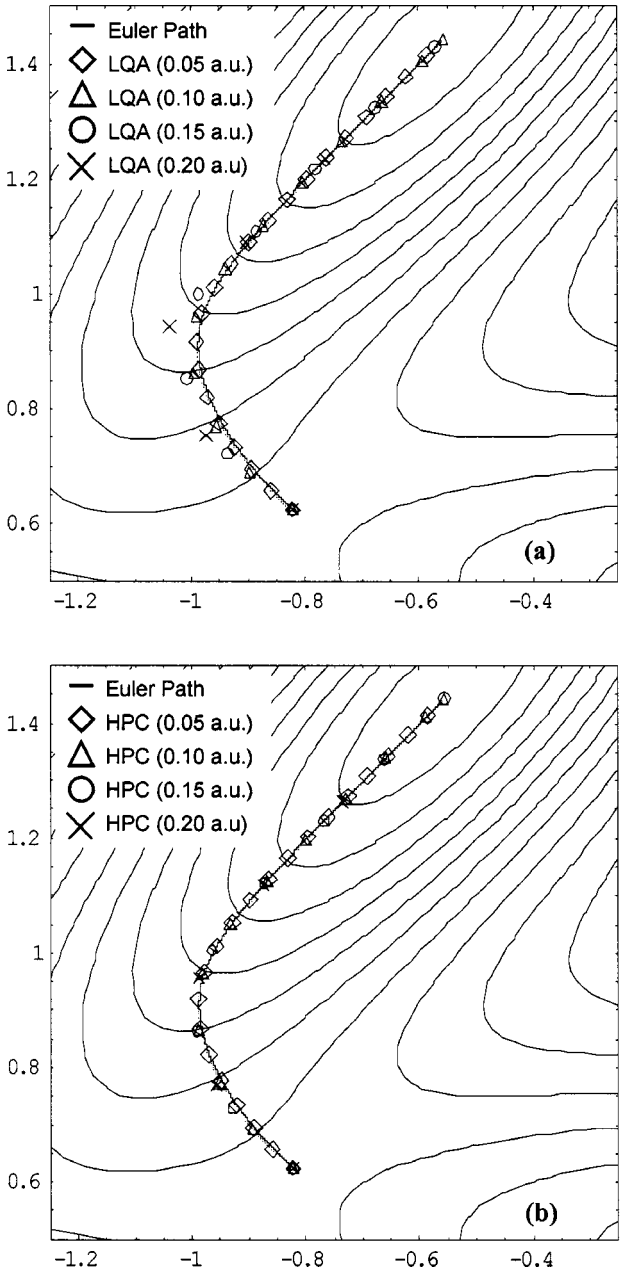

FIG. 2. Reaction path following on the Müller–Brown surface. Shown are contour diagrams of the surface and (a) LQA pathways and (b) HPC pathways using different step sizes.

B. HCN→HNC

The isomerization reaction of HCN is also often used to test new transition state searching and reaction path following algorithms. The present method was tested using this reaction's PES computed at the HF/STO-3G level of theory. The HPC paths were computed with several step sizes up to 0.400 a.u. All of the HPC pathways are superimposable and essentially identical. We have compared the HPC pathway computed with the largest step of 0.400 a.u. to the LQA pathway computed with a step size of 0.100 a.u., by calculating the perpendicular distance between the paths. A step size of 0.100 a.u. appears to be a practical upper limit for the LQA integrator.[17] The rms and maximum absolute perpendicular distance between the 0.400 a.u. step size HPC path

TABLE I. Perpendicular distances between LQA ($\Delta s = 0.10$ a.u.) and HPC ($\Delta s = 0.40$ a.u.) pathways for three reactions: HCN→HNC, the Diels–Alder reaction, and $CH_3CH_2F \rightarrow CH_2CH_2 + HF$.

Reaction	rms distance	max |distance|
HCN→HNC	4.67×10^{-4}	9.16×10^{-4}
Diels–Alder	7.86×10^{-4}	1.68×10^{-3}
$CH_3CH_2F \rightarrow CH_2CH_2 + HF$	9.73×10^{-4}	4.51×10^{-3}

and the 0.100 a.u. LQA path are reported in Table I. Table I also includes data for two other reactions (see below for discussion). As compared to the LQA pathway, the HPC integrator produces an identical plot (rms distance $<5\times10^{-4}$ bohr) even though a much larger step size is used. These data indicate the present method's stability and efficiency.

C. Diels–Alder reaction

The reaction of butadiene with ethene, the prototypical Diels–Alder reaction, has also been used to test the HPC method. Calculations were carried out at the AM1 level of theory. HPC calculations were carried out using step sizes up to 0.400 a.u. As before, the paths are all identical. We have tested the accuracy of the HPC method by measuring the perpendicular distance between the 0.400 a.u. HPC and 0.100 a.u. LQA paths. Table I shows that the HPC integrator does an excellent job of following the pathway, even with a large step size. Specifically, the rms perpendicular distance between these two pathways is 7.86×10^{-4} bohr.

D. $CH_3CH_2F \rightarrow CH_2CH_2 + HF$

The reaction of $CH_3CH_2F \rightarrow CH_2CH_2 + HF$ is a standard four center elimination process, which has been studied by Kato and Morokuma[41] and has been used in previous tests of reaction path following algorithms. *Ab initio* calculations were carried out at the HF/3-21G level of theory. Again, the HPC pathway was integrated with step sizes up to 0.400 a.u., and a LQA pathway was computed using a step size of 0.100 a.u. Table I shows the ability of the HPC integrator to accurately follow the IRC pathway. With a large step size (0.400 a.u.), the HPC pathway still follows the 0.100 a.u. LQA pathway very well, and the rms distance between these two paths is 9.73×10^{-4} bohr.

E. $Cl^- + CH_3Cl \rightarrow ClCH_3 + Cl^-$

Calculations at the HF/6-31G(d) level of theory were employed to study the symmetric S_N2 reaction of chloride with methyl chloride. This reaction is a good test case for reaction path following methods as it has been shown to be difficult to compute a highly accurate pathway in the area very near the TS.[42] The TS structure has significantly shorter C–H bonds. As a result, the symmetric C–H stretch frequency is strongly coupled to the reaction coordinate and the projected frequency associated with this normal mode is very sensitive to the quality of the steepest decent pathway integration. Very small deviations from the true IRC can produce erratic behavior from this frequency. As the previous work suggested,[42] we imposed very tight optimization criteria on the TS (i.e., rms gradient $<10^{-6}$ a.u., maximum gradient component $<2\times10^{-6}$, rms displacement $<4\times10^{-6}$ a.u. or rad, maximum displacement component $<6\times10^{-6}$ a.u. or rad). LQA and HPC integrations have been carried out using a step size of 0.010 a.u.

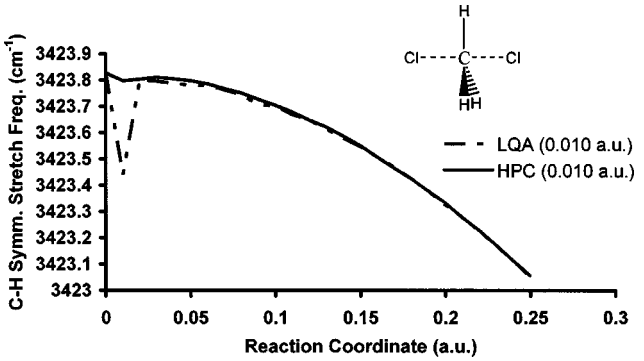

FIG. 3. Projected symmetric C–H stretch frequency vs reaction coordinate using the LQA and HPC integration methods. The structure of the transition state is also shown.

The projected symmetric C–H stretching frequencies for ca. 0.25 a.u. along the reaction coordinate are shown in Fig. 3. This plot should be smooth; however, the symmetric C–H stretch mode frequencies resulting from the LQA pathway have a deep minimum at 0.01 a.u. Following this minimum, the LQA path slowly recovers over subsequent steps. These errors are the direct result of slight displacements in the LQA pathway from the true reaction path in this region due to strong coupling of the reaction coordinate and this stretching mode near the TS.

The HPC pathway, on the other hand, corrects the errors in the LQA pathway, and the symmetric C–H stretch mode frequencies computed using the HPC pathway provide the expected smooth curve. Aside from a very shallow dip in the symmetric C–H stretch frequency at the first step, the HPC pathway provides an excellent description of the IRC and produces the expected smooth curve shown in Fig. 3. The predictor–corrector combination of methods in the present case offers a very stable integrator that is equivalent to the Gonzalez–Schlegel fourth order integrator.[22] The higher order method is better able to deal with the difficulties associated with the Eq. (1) stiff behavior near the TS.

F. Nickel metallacycle formation reaction

We have studied the ability of the HPC integrator to follow the reaction pathway of the oxidative cyclization step of a proposed mechanism for a nickel catalyzed three component addition reaction. This reaction has been studied extensively experimentally by Montgomery and co-workers,[43] and has recently been further investigated in a combined experimental and computational work.[44] The energy profile as a function of reaction coordinate using LQA and HPC is shown in Fig. 4. For both integrators a step size of 0.100 a.u. has been used. This process has a very late TS. Therefore, we have chosen to follow the pathway from the TS to the reactant well only. As shown in the figure, the LQA integrator takes a bad first step and heads up in energy. This indicates

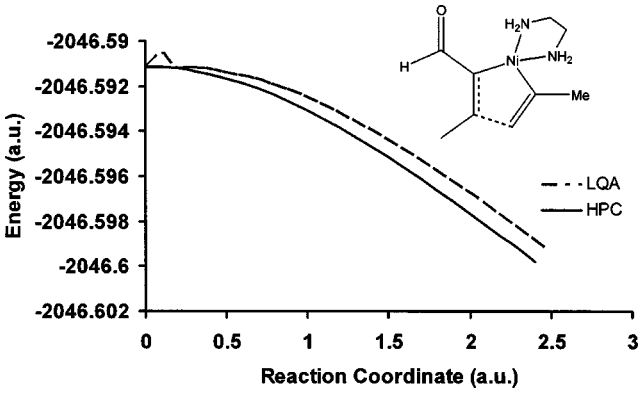

FIG. 4. Nickel metallacycle formation energy profile vs reaction coordinate using the LQA and HPC integration methods. The structure of the transition state is also shown.

that the reaction path is strongly curved at the TS. The HPC integrator is able to correct this poor step and continue down the path. This example displays HPC's ability to follow pathways involving large systems and to overcome significant errors in the predictor step.

IV. CONCLUSIONS

We have introduced a new Hessian based predictor–corrector (HPC) method for reaction path following. The HPC algorithm has been tested on the Müller–Brown surface as well as various chemical reactions. Additionally, we have studied the S_N2 reaction of chloride plus methyl chloride to demonstrate the ability of HPC to provide an accurate reaction path description that affords the expected smooth curve of the symmetric C–H stretch projected frequency as a function of reaction coordinate. This result is in contrast with that provided by a local quadratic approximation (LQA) pathway, which shows an erroneous sharp minimum in the curve.

ACKNOWLEDGMENTS

The authors extend thanks to S. Beier and J. L. Sonnenberg for helpful discussions. H.P.H. thanks the Institute for Scientific Computing at Wayne State University for support provided by a NSF–IGERT Fellowship. This work was supported by a grant from the NSF (CHE 0131157).

[1] D. G. Truhlar and B. C. Garrett, Annu. Rev. Phys. Chem. **35**, 159 (1984).
[2] D. G. Truhlar, B. C. Garrett, and S. J. Klippenstein, J. Phys. Chem. **100**, 12771 (1996).
[3] B. C. Garrett and D. G. Truhlar, in *Encyclopedia of Computational Chemistry*, edited by P. v. R. Schleyer, N. L. Allinger, P. A. Kollman, T. Clark, H. F. Schaefer III, J. Gasteiger, and P. R. Schreiner (Wiley, Chichester, 1998), Vol. 2, p. 3094.
[4] W. H. Miller, N. C. Handy, and J. E. Adams, J. Chem. Phys. **72**, 99 (1980).
[5] E. Kraka, in *Encyclopedia of Computational Chemistry*, edited by P. v. R. Schleyer, N. L. Allinger, P. A. Kollman, T. Clark, H. F. Schaefer III, J. Gasteiger, and P. R. Schreiner (Wiley, Chichester, 1998), Vol. 2, p. 2437.
[6] D. R. Alfonso and K. D. Jordan, J. Comput. Chem. **24**, 990 (2003).
[7] K. Fukui, Acc. Chem. Res. **14**, 363 (1981).
[8] M. L. McKee and M. Page, Rev. Comput. Chem. **4**, 35 (1993).
[9] H. B. Schlegel, in *Modern Electronic Structure Theory*, edited by D. R. Yarkony (World Scientific, Singapore, 1995).
[10] H. B. Schlegel, in *Encyclopedia of Computational Chemistry*, edited by P. v. R. Schleyer, N. L. Allinger, T. Clark, J. Gasteiger, P. A. Kollman, H. F. Schaefer III, and P. R. Schreiner (Wiley, Chichester, 1998), pp. 2432.
[11] M. A. Collins, Adv. Chem. Phys. **93**, 389 (1996).
[12] M. W. Schmidt, M. S. Gordon, and M. Dupuis, J. Am. Chem. Soc. **107**, 2585 (1985).
[13] K. Ishida, K. Morokuma, and A. Komornicki, J. Chem. Phys. **66**, 2153 (1977).
[14] K. K. Baldridge, M. S. Gordon, R. Steckler, and D. G. Truhlar, J. Phys. Chem. **93**, 5107 (1989).
[15] B. C. Garrett, M. J. Redmon, R. Steckler, D. G. Truhlar, K. K. Baldridge, D. Bartol, M. W. Schidt, and M. S. Gordon, J. Phys. Chem. **92**, 1476 (1988).
[16] M. Page and J. M. McIver, J. Chem. Phys. **88**, 922 (1988).
[17] M. Page, C. Doubleday, and J. W. McIver, J. Chem. Phys. **93**, 5634 (1990).
[18] K. Müller and L. D. Brown, Theor. Chim. Acta **53**, 75 (1979).
[19] J. Q. Sun and K. Ruedenberg, J. Chem. Phys. **99**, 5269 (1993).
[20] C. Gonzalez and H. B. Schlegel, J. Chem. Phys. **90**, 2154 (1989).
[21] C. Gonzalez and H. B. Schlegel, J. Phys. Chem. **94**, 5523 (1990).
[22] C. Gonzalez and H. B. Schlegel, J. Chem. Phys. **95**, 5853 (1991).
[23] H. B. Schlegel, J. Comput. Chem. **24**, 1514 (2003).
[24] C. W. Gear, *Numerical Initial Value Problems in Ordinary Differential Equations* (Prentice-Hall, Englewood Cliffs, NJ, 1971).
[25] V. Bakken, J. M. Millam, and H. B. Schlegel, J. Chem. Phys. **111**, 8773 (1999).
[26] J. M. Millam, V. Bakken, W. Chen, W. L. Hase, and H. B. Schlegel, J. Chem. Phys. **111**, 3800 (1999).
[27] R. Bulirsch and J. Stoer, Numer. Math. **6**, 413 (1964).
[28] R. Bulirsch and J. Stoer, Numer. Math. **8**, 1 (1966).
[29] R. Bulirsch and J. Stoer, Numer. Math. **8**, 93 (1966B).
[30] R. Farwig, Math. Comput. **46**, 577 (1986).
[31] R. Farwig, in *Algorithms for Approximation*, edited by J. Mason and M. Cox (Clarendon, Oxford, 1987), p. 194.
[32] M. A. Collins, Theor. Chem. Acc. **108**, 313 (2002).
[33] D. K. Hoffman, R. S. Nord, and K. Ruedenberg, Theor. Chim. Acta **69**, 265 (1986).
[34] W. H. Press, *Numerical Recipes in FORTRAN 77: The Art of Scientific Computing*, 2nd ed. (Cambridge University Press, Cambridge, 1996).
[35] V. S. Melissas, D. G. Truhlar, and B. C. Garrett, J. Chem. Phys. **96**, 5758 (1992).
[36] R. P. A. Bettens and M. A. Collins, J. Chem. Phys. **111**, 816 (1999).
[37] K. C. Thompson, M. J. T. Jordan, and M. A. Collins, J. Chem. Phys. **108**, 564 (1998).
[38] J. Ischtwan and M. A. Collins, J. Chem. Phys. **100**, 8080 (1994).
[39] P. Lancaster and K. Salkauskas, *Curve and Surface Fitting: An Introduction* (Academic, London, 1986).
[40] M. J. Frisch, G. W. Trucks, H. B. Schlegel *et al.*, Gaussian 03, Development Version, Revision B.04, Gaussian, Inc., Pittsburgh, PA, 2003.
[41] S. Kato and K. Morokuma, J. Chem. Phys. **73**, 3900 (1980).
[42] A. G. Baboul and H. B. Schlegel, J. Chem. Phys. **107**, 9413 (1997).
[43] J. Montgomery, Acc. Chem. Res. **33**, 467 (2000).
[44] H. P. Hratchian, S. K. Chowdhury, V. M. Gutiérrez-Garcia, H. B. Schlegel, and J. Montgomery (unpublished).